(Received 22 July 2025, Accepted 30 September 2025, Scheduled 14 October 2025)

Reconfigurable Designs of U-Slot Cut Microstrip Antennas for Dual Band Circularly Polarized Response

Amit A. Deshmukh[1] and Venkata A. P. Chavali[2,*]

[1] *Department of EXTC, SVKM's DJSCE, Mumbai, India*
[2] *Department of ECE, IIIT Surat, Surat, India*

ABSTRACT: Resonant slot cut microstrip antenna is a single patch solution to achieve circularly polarized response, but it does not offer tunability in the center frequency of axial ratio bandwidth. This paper presents reconfigurable designs of shorting post loaded U-slot cut circular and equilateral triangular microstrip antennas that offer tunable circularly polarized response. Shorting posts positions alter the excitation of resonant modes on the U-slot cut patch that achieves tuning in the circularly polarized frequency. On the substrate thickness of $\sim 0.05\lambda_{cAR}$, using the circular patch, tuning in the center frequency of axial ratio bandwidth by 253 MHz (28.26%) is obtained, whereas equilateral triangular patch design offers 319 MHz (32.68%) of frequency tuning. In both the designs, broadside radiation pattern with a peak gain of larger than 7 dBic is obtained across the axial ratio bandwidth. Design methodology is proposed that yields a similar configuration as per specific wireless application. With the obtained frequency tuning in axial ratio bandwidth, redesigned variations of the proposed configurations can cater to pairs of GPS L-band applications.

1. INTRODUCTION

Microstrip antenna (MSA) finds maximum applications in wireless communication due to their advantages like low profile planar design [1, 2]. In these applications, signal undergoes multi-path propagation effects, due to which polarization of the incident signal at the receiver cannot be certain. To avoid the signal loss arising from the polarization mismatch, circularly polarized (CP) antennas are selected at the receiver. In MSA, CP response is obtained by employing suitable modifications in the patch or the ground plane. Various techniques to achieve this are narrow slot cut patch excited using coaxial feed, open circuit stubs placed on the patch edges, use of shorting posts, modified shape of the radiating patch, resonant slot loaded configurations, and use of modified ground plane structures in the form of slots or fractal geometries [3–14]. These CP designs either employ thinner efficient microwave substrate or air suspended substrate. The use of air suspended substrate in resonant slot cut CP MSA improves the reliability in antenna results against the substrate parameter variations and also provides a low-cost solution. Wideband CP MSAs are required when multiple adjoining wireless bands are catered to using a single antenna, e.g., GPS L and Galileo E-bands. In these designs, axial ratio (AR) bandwidth (BW) of more than 10% is needed. The wideband CP MSAs are realized either by employing parasitic resonators in the gap-coupled or stacked layer, or by employing non-contact microstrip line feeding technique exciting multiple patches or by cutting multiple resonant slots inside the patch [15–22]. These wideband MSAs yield AR BW in the range of 10–25%, but they exhibit variation in the broadside gain over the AR or reflection coefficient (S_{11}) BW. Also, with the multiple patches, antenna size is large. Instead of employing wideband CP MSA, dual or triple band CP MSAs can be used for catering to adjoining frequency spectrums of given wireless application, e.g., GPS L1, L2, L5 bands. The multi-band CP response is obtained by cutting resonant slots inside the patch or by employing modified patch shapes [23–26, 30]. However, these designs either require thicker substrate or larger patch size, and offer lower peak gain. The triple band circular patch design for GPS L5, L2, and L1 bands is reported in [27]. It employs four feed network, thus increasing the complexity for the feed design. By employing reconfigurable approach, tuning in the center frequency of AR BW is obtained [28, 29]. But in these designs, broadside antenna gain does not remain constant across the tuning range.

In terms of low cost suspended substrate and its thickness (0.07–$0.08\lambda_g$), resonant slot cut CP MSA is an optimum single patch solution for the obtained AR BW (3–6%) and broadside gain (6–8 dBic). The drawback of this design is that it does not offer tuning in the center frequency of AR BW, which is required in frequency agile and multi-band applications. The present work addresses this research gap, and using the reconfigurable approach, dual band configurations of coaxially fed resonant U-slot cut circular MSA (CMSA) and equilateral triangular MSA (ETMSA) are proposed in this paper. The antennas are presented using a three-layer suspended configuration, which consists of two FR4 substrate ($\varepsilon_r = 4.3$, $h = 0.16$ cm) layers separated by an air gap of h_a cm. Initially, CMSA and ETMSA dimensions were optimized for the fundamental mode frequency around 1000 MHz, on the total substrate thickness of $\sim 0.06\lambda_g$. Here, λ_g refers to wavelength in the suspended

* Corresponding author: Venkata A. P. Chavali (cpriyag14@gmail.com).

substrate at the fundamental mode. Further, respective designs were optimized with a U-slot to obtain the dual band response with CP characteristics in the first band. On the total substrate thickness of $\sim 0.055\lambda_{cAR}$, U-slot cut CMSA yields simulated BWs of 66 MHz (7.15%) and 84 MHz (6.47%) in two bands with AR BW of 23 MHz (2.48%) in the first band. As the paper deals with CP antennas, substrate thickness is mentioned in terms of wavelength at the center frequency of AR BW (λ_{cAR}). In U-slot cut CMSA, diagonally directed resonant modes are present, which are responsible for the CP response. Hence, to tune the center frequency of AR BW, parametric study for the placement of shorting posts around the perimeter of circular patch is carried out. The shorting posts positions alter the resonance frequencies and surface current distribution at excited orthogonal modes which achieves tuning in the AR BW frequency. An optimum response in terms of frequency tuning is obtained for shorting posts placed along $\alpha = 45°$. To realize this frequency tuning practically, reconfigurable design is selected, wherein radio frequency (RF) PIN diodes were used to realize the shorting of the CMSA along the patch perimeter. In shorting posts loaded U-slot cut CMSA, with the activation of PIN diodes, the center frequency of AR BW increases from 895 MHz to 1148 MHz, thereby providing 253 MHz (28.26%) of frequency tuning. The radiation pattern remains in the broadside direction in the two operating bands with a broadside gain of more than 7 dBic. With the loading of shorting posts and subsequent activation of PIN diodes, antenna offers dual band response, similar to the initial U-slot cut CMSA. A similar study is carried out for the CP design of U-slot cut ETMSA for the placement of shorting posts along the vertex points and variation of their positions along the ETMSA base, as explained below. In this, optimum response in terms of frequency tuning is achieved for shorting posts placed at the three vertex points. The practical implementation is realized using the reconfigurable approach, and the suitable excitation of PIN diodes achieves AR BW center frequency tuning from 976 MHz to 1295 MHz (319 MHz, 32.68%). In both the responses for PIN diode activation, dual band response with broadside radiation pattern and a peak gain of more than 7 dBic is obtained. In both the reconfigurable U-slot cut designs, for the substrate thickness around $\sim 0.055\lambda_{cAR}$, AR BW in the range of 1.5–2.5% is obtained. Lastly, resonant length formulation at U-slot cut patch modes and subsequent design methodology is presented. The U-slot cut reconfigurable CMSA and ETMSA designed using this methodology yield frequency tunable response to cover either L1, L2 or L1, L5 bands, respectively. Although the resonant U-slot cut CP MSA is a well reported design, the same does not provide tuning in the center frequency of AR BW, and hence it is not useful in frequency agile and multi-band applications. Current study does not just present another U-slot cut CP design but presents a frequency tunable design that addresses the above research gap and makes it suitable in frequency agile, multi-band applications. In this frequency tuning capability, proposed shorted reconfigurable configuration is novel in terms of the technique used and results obtained. The proposed designs were initially optimized using Computer Simulation Technology (CST) software [31] followed by experimental verifications. A good degree of agreement is obtained between the simulated and measured results.

2. RECONFIGURABLE DESIGN OF U-SLOT CUT SHORTED CMSA FOR CP RESPONSE

The coaxially fed CMSA embedded with a U-slot is shown in Figs. 1(a), (b). In the suspended design, two layers of FR4 substrate are used, separated by an air gap thickness of h_a cm. The patch is fabricated on top FR4 layer, whereas ground plane is realized on the bottom FR4 layer. For $h_a = 1.4$ cm, CMSA radius 'r' is parametrically optimized using the simulations for TM_{11} mode frequency of 950 MHz. 'r' is found to be 6.5 cm, for the total substrate thickness of 1.72 cm ($0.059\lambda_g$). While employing the parametric study for U-slot dimensions, L_h, L_{h1}, L_v, and w_u, a dual band response in U-slot cut CMSA is obtained. It provides simulated BW for $S_{11} \leq -10$ dB of 66 MHz (7.15%) and 84 MHz (6.47%) in the two bands with AR BW of 23 MHz (2.48%) in the first band. Since the paper addresses the CP designs, the total substrate thickness is now expressed in terms of the wavelength at the center frequency of AR BW (927 MHz) as $0.058\lambda_{cAR}$. The CP response in the first band is attributed to the optimum inter-spacing between the degenerated and diagonally ($\alpha = 45°$) directed TM_{11}^{45} and TM_{11}^{135} modes [33], as shown in Figs. 1(d), (e). The second band response is attributed to the modified TM_{21} mode [33], as shown in Fig. 1(f). To tune the AR BW center frequency, frequencies of TM_{11}^{45} and TM_{11}^{135} modes should be changed together. A technique of achieving the same is by placing equal lengths open circuit stubs at $\alpha = 45°$, along all the sides of the patch perimeter, as given in Fig. 1(a). However, the placement of stubs alters the impedance variation on the slot cut patch that does not achieve the CP response for $S_{11} \leq -10$ dB. Therefore, effects of placing the shorting posts along all the sides on the patch perimeter at an angle 'α', as shown in Fig. 1(a), are studied. The shorting posts are loaded on the patch as mentioned in Figure 1. Parametric variations are carried out for an increase in 'α'. Respective resonance curve, AR plots, and the surface current distribution at observed resonant modes are given in Figs. 2 & 3.

Without the loading of shorting posts, resonant modes in the design are those of the U-slot cut CP CMSA, i.e., TM_{11}^{45}, TM_{11}^{135}, and modified TM_{21} modes. With the placement of shorting posts, resonant modes in the shorted antenna cavity and relevant surface current distribution change. At lower angles, surface current distribution at the first observed resonant mode is varied prominently along the horizontal direction inside the U-slot cut CMSA, hence the mode is referred to as TM_{10}. Here, some contribution of vertically directed surface currents does exist, but largely the currents are horizontally directed. The TM_{10} mode frequency increases by a small margin with angle 'α'. The resonant mode identification for shorted U-slot cut CMSA is carried out purely based on the surface current variation present along the two coordinate axes in the patch. Here, the same procedure is adapted for modal identification in conventional rectangular MSA as described in the literature [1–3]. At the next resonant mode, surface currents vary along vertical direction inside the shorted U-slot cut CMSA, and thus the

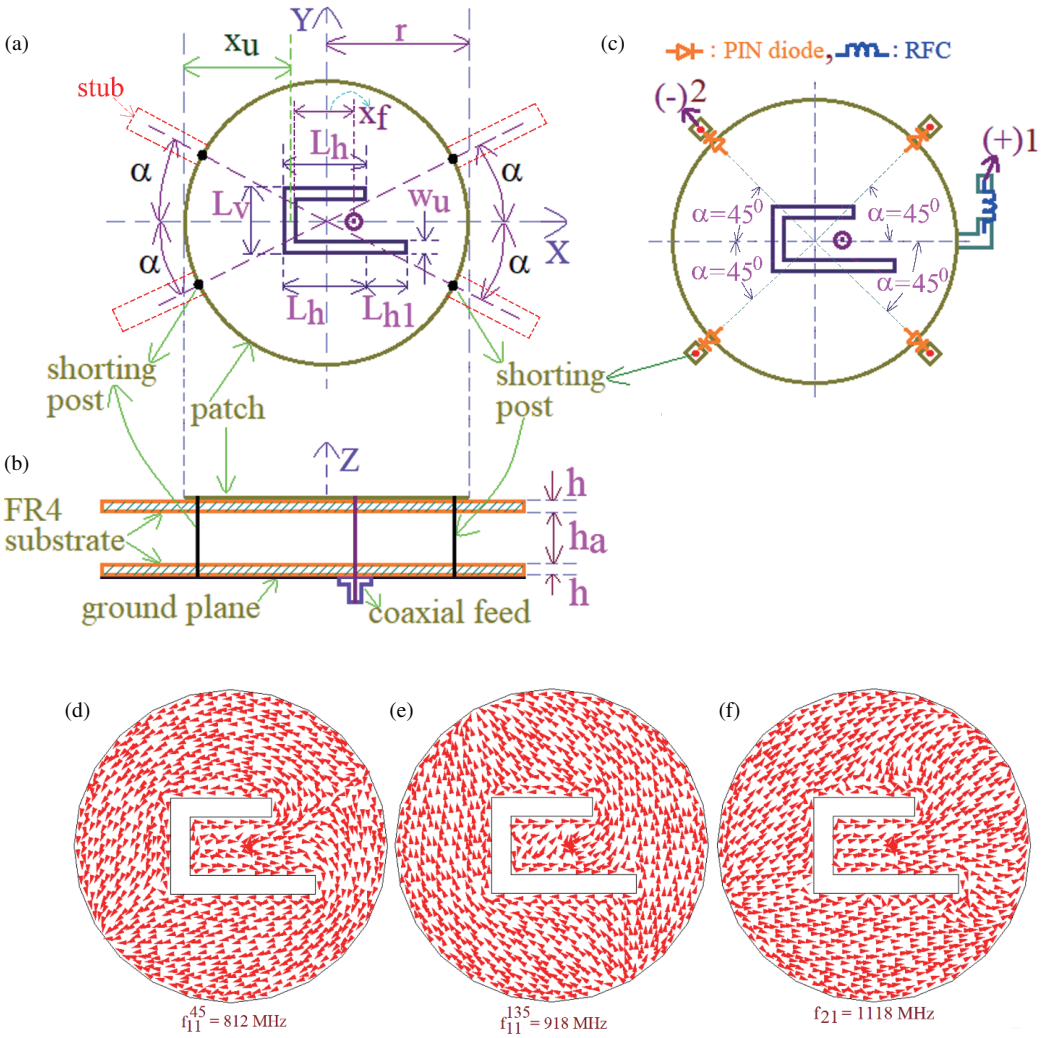

FIGURE 1. (a), (b) U-slot cut CMSA loaded with shorting posts, its (c) reconfigurable design, and (d)–(f) surface current distribution at observed resonant modes for dual band U-slot cut CMSA.

mode is identified as TM_{01}. This frequency shows higher increment in its value for α increasing from 15° to 45°. For $\alpha > 50°$, resonant mode distribution on the shorted patch changes. The first mode remains TM_{10} as surface currents vary along the horizontal direction inside the shorted slot cut CMSA. At the second mode, surface currents vary along the horizontal direction only, but the direction of currents is reversed to that present at TM_{10} mode. Due to this, modal identification for this mode is not explicitly stated. At the third mode, currents vary along vertical direction inside the shorted patch, and its frequency is closer to the modified TM_{21} mode frequency. As seen from AR plots, axial ratio values near and below 3 dB are observed for $\alpha \geq 45°$. But for $\alpha \geq 60°$, impedance at resonant modes is higher, where AR less than 3 dB is observed. This does not achieve $S_{11} \leq -10$ dB BW, to support AR ≤ 3 dB CP BW. Thus, optimum frequency tunable CP response for AR ≤ 3 dB supported with $S_{11} \leq -10$ dB is obtained only for $\alpha = 45°$. This CP response is attributed to the orthogonal surface current components on the patch at TM_{01} mode [13, 29], as shown in Fig. 3(e). Thus, without the shorting post, the center frequency of AR BW in U-slot cut CMSA is 927 MHz that increases to around 1150 MHz with the shorting posts loading.

For the practical realization of un-shorted and shorted conditions using U-slot cut CMSA, reconfigurable design is adapted as shown in Fig. 1(c). The shorting post is placed on the square shorting pad of length 0.2 cm, which is kept at an angle $\alpha = 45°$ with respect to the feed point axis. The connection of shorting post with the patch is achieved through the RF PIN diode 'BAR64-06W H6327'. The DC biasing of PIN diodes is realized using the RF choke (RFC) 'ELT-3KN131B', as shown in Fig. 1(c). When the positive supply is connected at (1) with negative polarity present at (2) as mentioned in Fig. 1(c), all the PIN diodes are forward biased. When diodes are in ON state, they offer minimal forward resistance (R_F) of 3.4 Ω, thereby providing the shorting between the circular patch and shorting posts. This realizes the configuration of U-slot cut CMSA loaded with shorting posts that achieves CP response in higher frequency band. When DC supply is not connected, the PIN diodes are in OFF state. In this condition, PIN diode is represented by the parallel combination of capacitor C and resistor R_P of values 0.25 pF and 3.2 kΩ, as shown in Fig. 4(a). At the

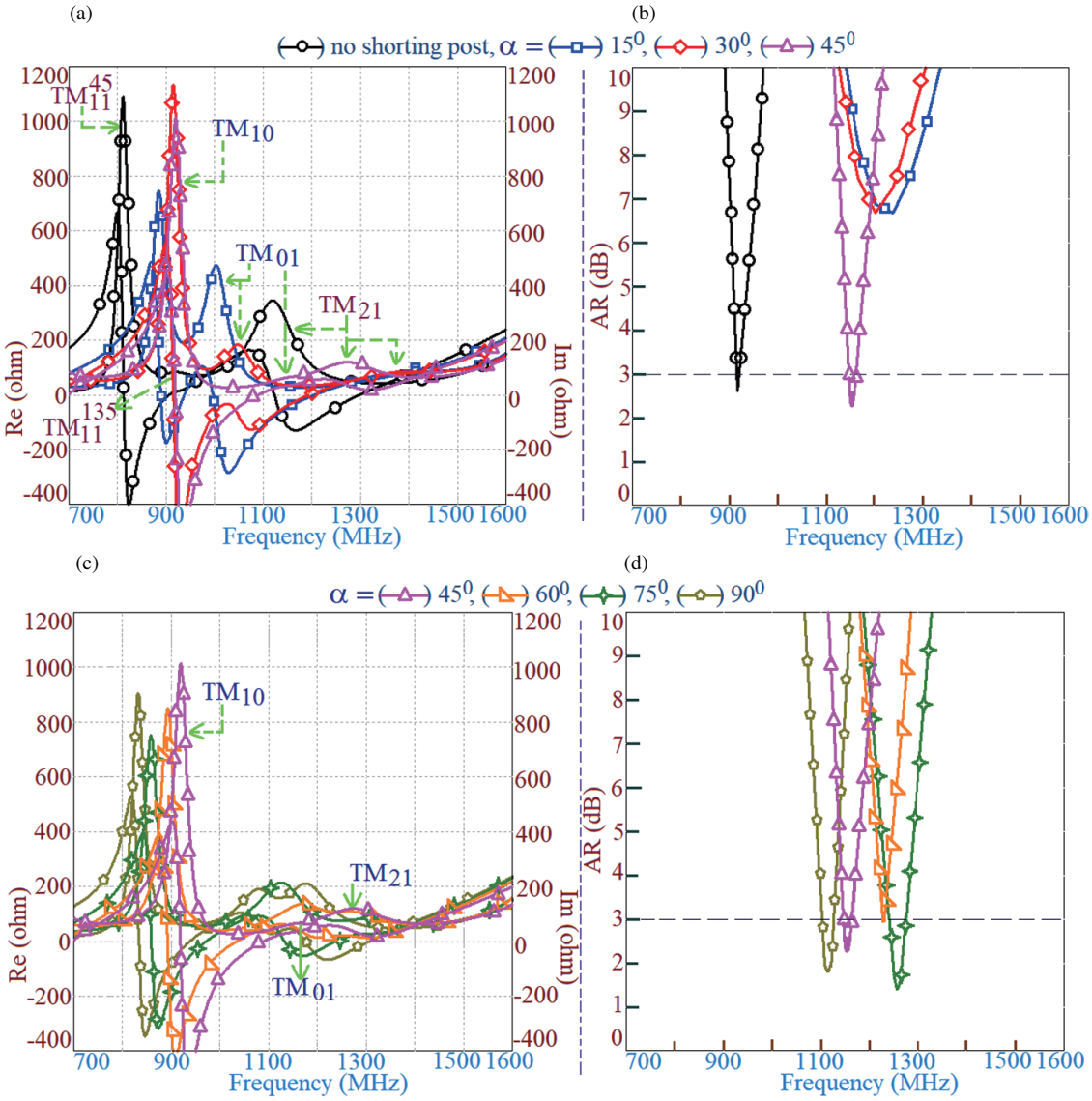

FIGURE 2. (a)–(d) Resonance curve and AR plots for U-slot cut CMSA against shorting posts position.

operating frequency, these elements ensure open circuit condition between respective shorting pads and circular patch and achieve the CP response in the lower frequency region. Series inductance L_s in the equivalent circuit equals 1.4 nH.

The reconfigurable designs were simulated, and their response is experimentally verified. For the antenna parameters as $r = 6.5$, $h_a = 1.4$, $h = 0.16$, $L_v = 4.0$, $L_h = 4.2$, $L_{h1} = 1.8$, $w_u = 0.8$, $x_f = 2.5$, $x_u = 4.4$ cm, results for the reconfigurable U-slot cut CMSA in the two activation states of PIN diodes are shown in Figs. 4 and 5. When the diodes are not forward biased, S_{11} BWs observed in the first band in the simulation and measurement are 58 MHz (6.5%) and 68 MHz (7.64%), respectively. The simulated and measured S_{11} BWs observed in the second band are 72 MHz (5.6%) and 84 MHz (6.5%), respectively. The AR BWs noted in the first band for the simulation and measurement are 22 MHz (2.45%) and 25 MHz (2.82%), respectively. The center frequency of AR BW observed in the simulation is 895 MHz. A slight reduction in this frequency as compared with the initial U-slot cut CP CMSA is attributed to the loading of shorting posts around the perimeter of the circular patch. The radiation pattern at the center frequency of AR BW shows right hand CP (RHCP) components greater in magnitude than the left hand CP (LHCP) components, thereby showing the presence of RHCP wave. Radiation pattern at the center frequency of the second band shows broadside radiation with cross-polar component less than 10 dB down as compared with the co-polar radiation level, thus ensuring a linear polarized response. The E-plane of radiation is directed along $\Phi = 0°$, across the second band.

With forward biasing of PIN diodes, shorting posts are connected with a circular patch, and the CP response is achieved in the higher frequency band. For this configuration, simulated values of S_{11} BW obtained in dual bands are 101 MHz (9.1%) and 57 MHz (4.23%), respectively. The corresponding measured values are 107 MHz (9.69%) and 59 MHz (4.35%), respectively. The simulated and measured values of AR BW

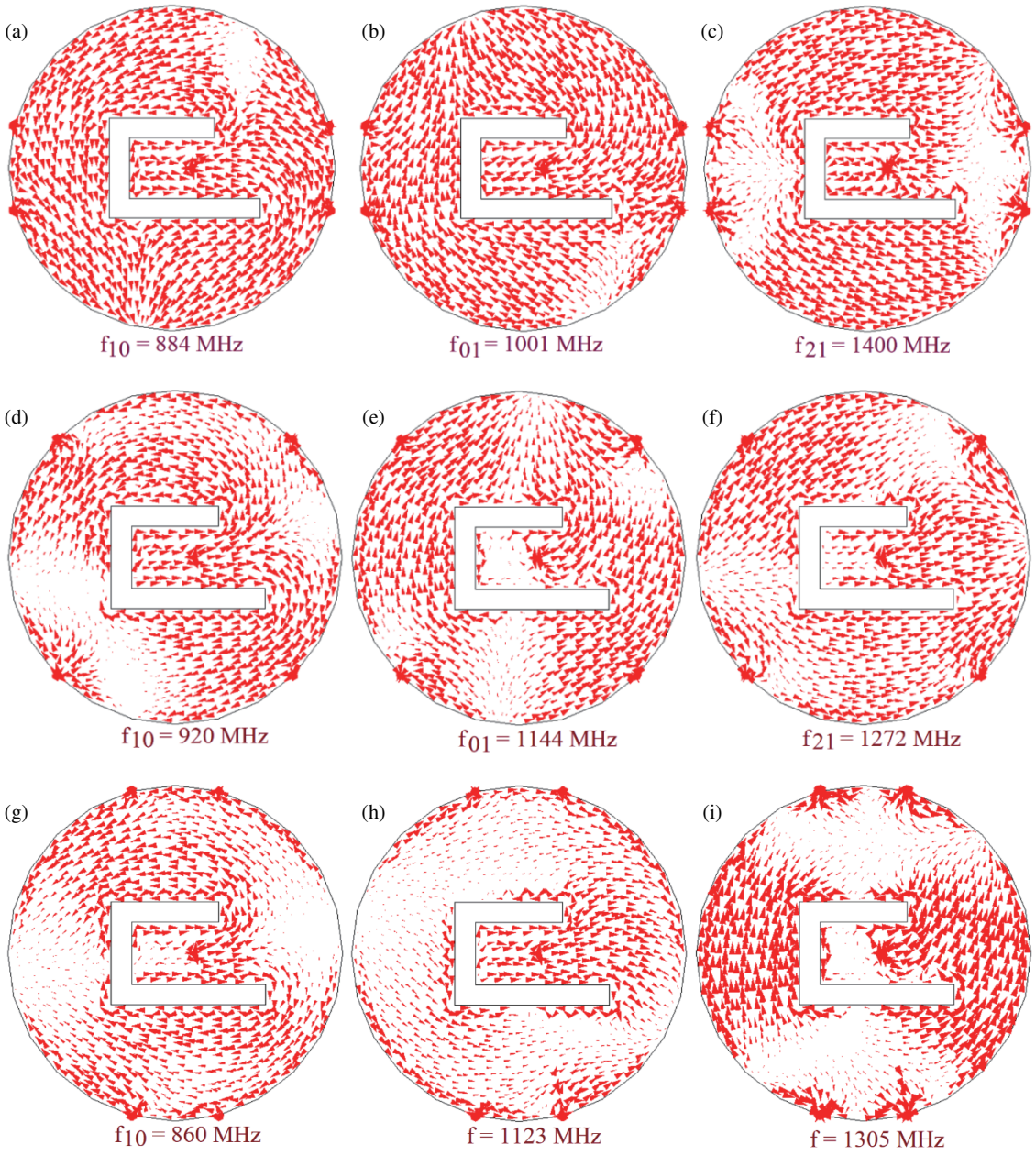

FIGURE 3. Surface current distribution at observed resonant modes for shorting posts loaded U-slot cut CMSA for α = (a)–(c) 15°, (d)–(f) 45° and (g)–(i) 70°.

as observed in the first band are 16 MHz (1.39%) and 15 MHz (1.31%), respectively. The center frequency of AR BW observed in the simulation is 1148 MHz. Thus, with the activation of PIN diodes, AR BW center frequency tuning by 253 MHz (28.26%), i.e., from 895 to 1148 MHz, is obtained. The % tuning is calculated with respect to the initial frequency, since the U-slot cut CMSA without the shorting post is the initial design. This % tuning range is quite large so as to cater to any practical wireless applications requiring dual band antennas. This frequency tuning design feature is not present in the reported CP designs of U-slot cut CMSA, and in this regard, proposed technique and configuration are novel in contribution. The S_{11} BW measurement for the proposed designs is carried out using vector network analyzer, ZVH-8. The biasing of the PIN diodes is achieved through the DC power supply connection as shown in Fig. 6(a). The radiation pattern and broadside gain are measured inside the antenna laboratory, and the setup for them is provided in Figs. 6(b), (c). In the pattern measurement for CP response, initially the measurement is carried out in two orthogonal planes, and further by using conversion equations, right and left hand field polarization components are evaluated [32]. The far-field distance is calculated with reference to the highest frequency of the measurement and for the present design, and the distance maintained is 300 cm. A reference wideband and high gain linear polarized horn antennas are used in these far-field measurements. Around the measurement desk, metallic objects are absent. Also the distance of the surrounding walls with respect to the measurement desk is more than seven

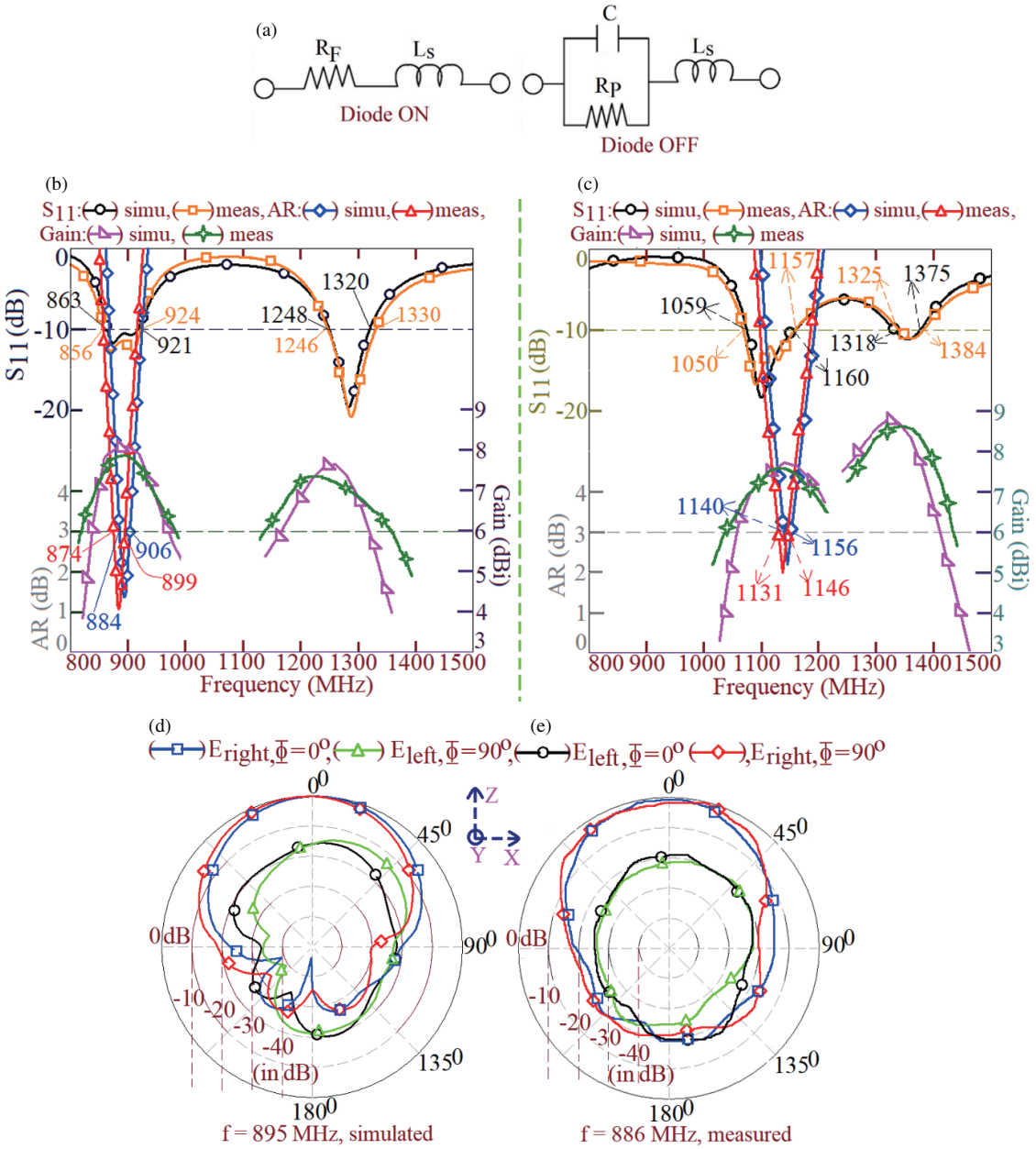

FIGURE 4. (a) Equivalent circuit of PIN diode, optimum results for reconfigurable U-slot cut CMSA in diode, (b) OFF and (c) ON state, (d), (e) field polarization plots at the center frequency of AR BW when PIN diodes are OFF.

times of the wavelength, calculated with reference to the lowest frequency of measurement. All these measurement details provide minimum possible reflection environment and fairly good match with reference to the ideal measurement carried out inside the anechoic chamber.

To confirm the CP radiation from the reconfigurable dual band U-slot cut CMSA over the two bands, orthogonal E-fields and their phase variation over the frequencies were studied. The CST model and respective plots are shown in Figs. 7(a)–(c). As can be seen, when diodes are in OFF state, CP response is obtained around 900 MHz band, where the magnitudes of E-fields are nearly the same with phase ϕx component leading ϕy by 90°. When PIN diodes are ON, the CP response is observed around 1150 MHz band, where orthogonal field magnitudes are nearly the same with ϕy component leading ϕx by 270°. Both of these phase differences confirm the presence of RHCP radiation with reference to transmitting antenna, across the two tunable bands. For the proposed reconfigurable U-slot cut CMSA, LHCP radiation in both the bands are obtained while selecting the upper arm horizontal U-slot length greater in dimension than the lower arm, as shown in Fig. 1(a).

3. RECONFIGURABLE DESIGN OF U-SLOT CUT SHORTED ETMSA FOR CP RESPONSE

The design of U-slot cut ETMSA for CP response is shown in Figs. 8(a), (b). The antenna is fabricated in a three-layer suspended configuration with an air gap of thickness h_a cm,

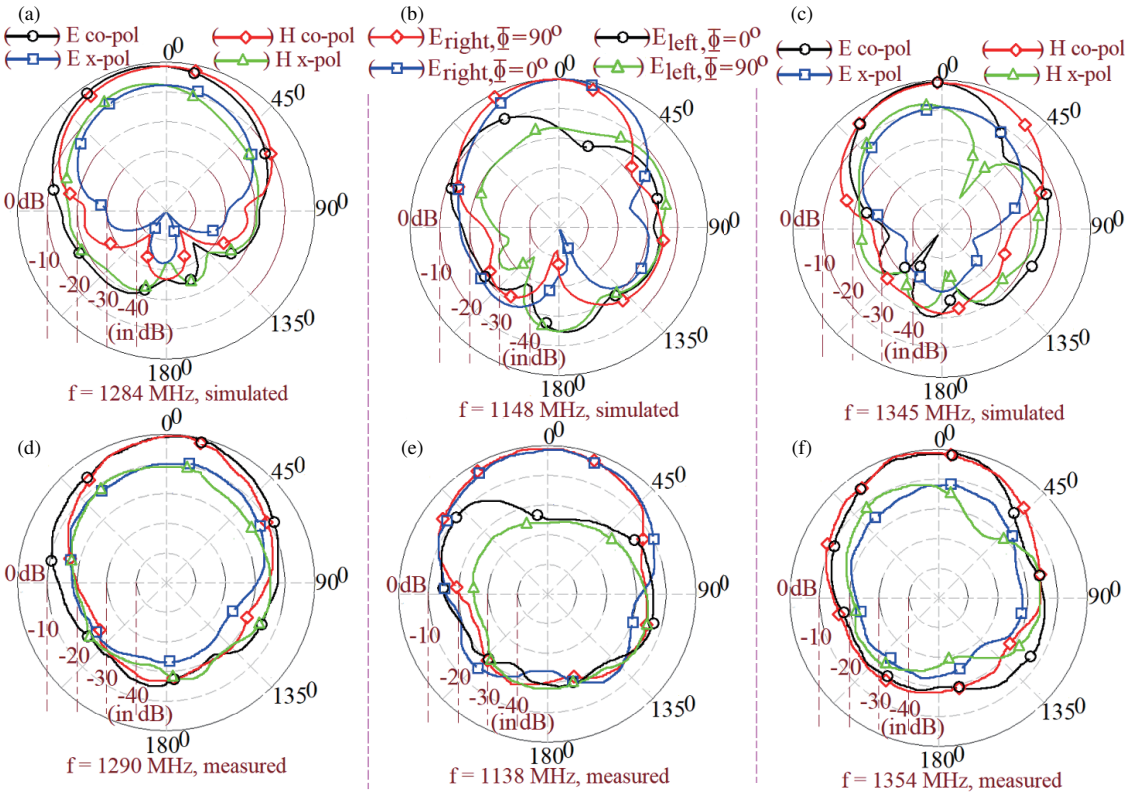

FIGURE 5. (a), (b) Radiation pattern plots at the center frequency of second band when PIN diodes OFF, (c), (d) field polarization plots at the center frequency of AR BW and (e), (f) radiation pattern plots at the center frequency of second band when PIN diodes are ON for U-slot cut CMSA.

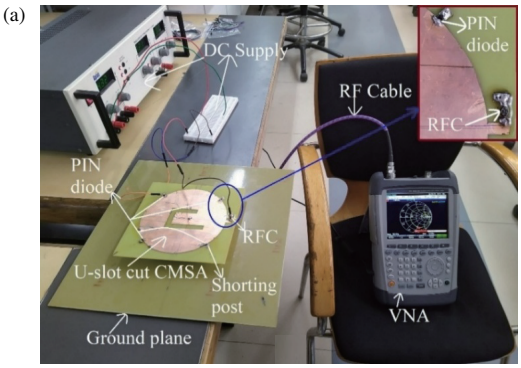

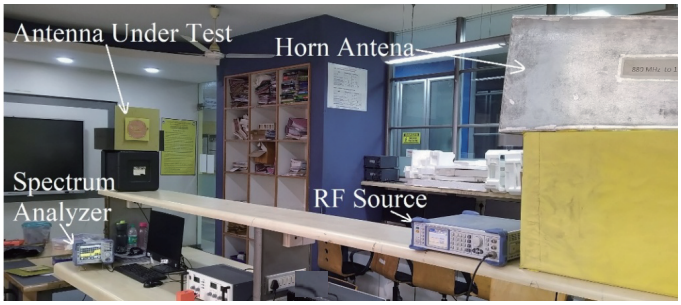

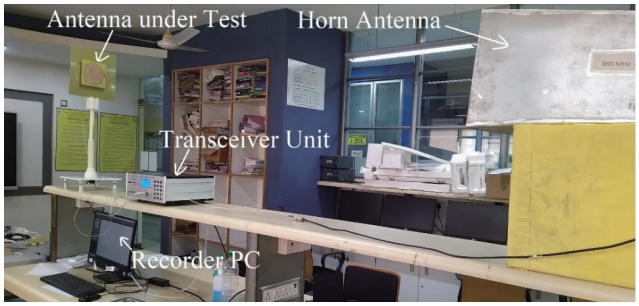

FIGURE 6. (a) S_{11} BW measurement setup, and (b) broadside gain, and (c) radiation pattern measurement setup for reconfigurable design of U-slot cut CMSA.

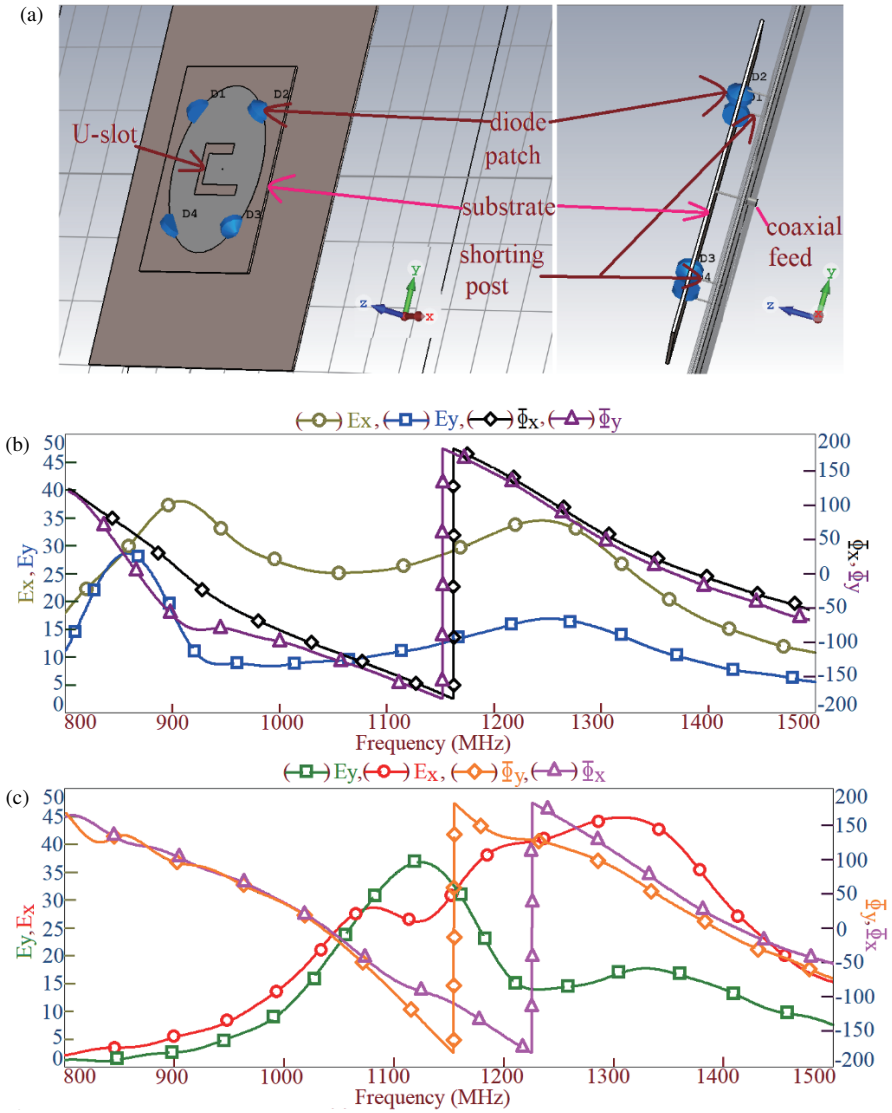

FIGURE 7. (a) CST model and orthogonal E-field magnitude and phase plots for PIN diodes in (b) OFF and (c) ON state, for reconfigurable U-slot cut CMSA.

between the two FR4 layers. In this design, side length 'S' is taken equal to 13 cm, i.e., equal to CMSA diameter selected above.

For this side length and $h_a = 1.2$ cm, the fundamental mode frequency (TM_{10}) of ETMSA is found to be 1041 MHz, which gives an electrical substrate thickness of $0.058\lambda_g$. This thickness is the same as that present in CMSA design. Inside this ETMSA and with reference to TM_{10} mode null field line as shown in Fig. 8(a), the U-slot is cut. Using the parametric optimization, dual band response with CP characteristics in the first band is achieved in U-slot cut ETMSA. For the antenna parameters as $S = 13$, $h_a = 1.2$, $h = 0.16$, $L_h = 3.5$, $L_{h1} = 1.4$, $L_v = 3.4$, $x_f = 1.9$, $x_u = 2.2$ cm, simulated S_{11} BWs observed in the dual bands are 77 MHz (7.61%) and 89 MHz (5.58%), respectively. The simulated AR BW noted in the first band is 22 MHz (2.19%). In this design also, CP response is attributed to the degenerated TM_{10} modes [33], i.e., TM_{10}^{45}, TM_{10}^{135}, along the two diagonal axes, as shown in Figs. 8(d), (e). The second band response is due to the modified TM_{11} mode [33] as shown in Fig. 8(f). As the resonant mode currents contributing to the AR BW show diagonal variation inside the U-slot cut ETMSA, effects of placing the shorting posts on the patch vertex points and subsequently their offset positions (y_s) are studied as shown in Fig. 8(a). Initially, shorting posts are placed at the vertex point, i.e., $y_s = 0$, and then y_s is increased in steps. Effects of these variations on the resonant mode excitation and input impedance at them, AR variation, and surface current distribution at observed modes are provided in Figs. 9(a)–(k).

Without the shorting posts, AR BW is formed in 1000 MHz spectrum, i.e., as given by U-slot cut ETMSA. When the shorting posts are loaded at the vertex point, the excitation of resonant mode changes. At the first of the observed resonant modes, surface currents vary along horizontal axis inside the shorted U-slot cut ETMSA as shown in Fig. 9(c). With this variation, mode is referred to as TM_{10}. At the second mode,

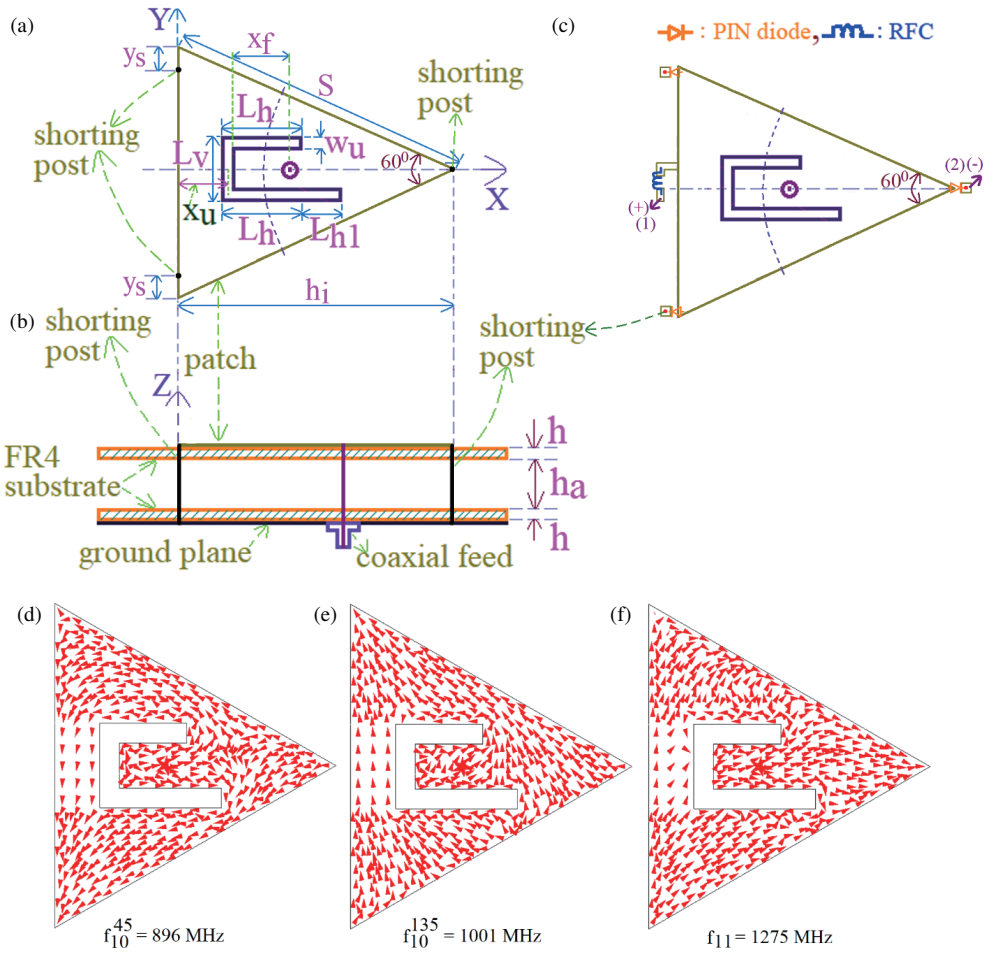

FIGURE 8. (a), (b) U-slot cut ETMSA loaded with shorting posts, and its (c) reconfigurable design, (d)–(f) surface current distribution at observed resonant modes for U-slot cut ETMSA.

surface currents vary along vertical direction inside the patch, as shown in Fig. 9(d), and hence the same is referred to as TM_{01}. At this mode surface current components show orthogonal variation over the patch that leads to the AR value less than 3 dB towards those frequencies [13, 29]. This AR value is supported with input impedance less than 100 Ω, thereby yielding $S_{11} \leq -10$ dB, over those frequencies. Thus with the shorting post at the vertex point, tuning in the AR BW center frequency with respect to un-shorted design is achieved. The next resonant mode observed for the shorting posts at the patch vertex, is modified TM_{11}, which is similar to that observed for U-slot cut ETMSA without the shorting posts loading. With an increase in y_s, two of the shorting posts are placed away from the vertex point. With an increment in y_s from 0 to 2 cm, TM_{10} mode frequency changes by a small margin, whereas TM_{01} mode frequency remains constant. For this shorting position also, antenna offers CP response with AR < 3 dB, for $S_{11} \leq -10$ dB as shown in Figs. 9(a), (b). The center frequency of CP BW is marginally changed with respect to shorting posts at the vertex points. For $y_s = 2.0$ cm, AR < 3 dB is also observed in the lower frequency region. However, an input impedance matching to realize $S_{11} \leq -10$ dB, at this frequency is not obtained. With further increment in y_s, TM_{10} mode frequency changes by a small amount, but TM_{01} mode frequency decreases. An input impedance at the same also increases that does not realize CP characteristics for AR < 3 dB. Thus, CP characteristics with a frequency tuning is obtained for $y_s = 0$ and 2 cm.

With these findings, the reconfigurable design of U-slot cut ETMSA is realized. For this, shorting posts are placed on square shorting pads of length 0.2 cm, which are placed in the close vicinity of the U-slot cut ETMSA. The reconfigurable designs for $y_s = 0$ and 2.0 cm were separately simulated with the shorting posts placed on the pads. The effects of placement of shorting post on the patch edge against that on the shorting pads are different in terms of frequency and input impedance at the degenerated orthogonal modes. In this study, it was noted that reconfigurable CP response in the higher frequency range for AR < 3 dB was not realized for $y_s = 2$ cm. Therefore, reconfigurable design is only realized for $y_s = 0$ cm, as shown in Fig. 8(c). The shorting pads are connected to the U-slot cut ETMSA through the PIN diodes for the polarity shown. The biasing of these PIN diodes is achieved through the RFC as shown in Fig. 8(c). With the positive polarity of DC bias in (1) and the negative polarity in (2), all the PIN diodes are forward biased, and the CP response is obtained in higher frequency region as shown in Fig. 9(b). When the DC bias is not con-

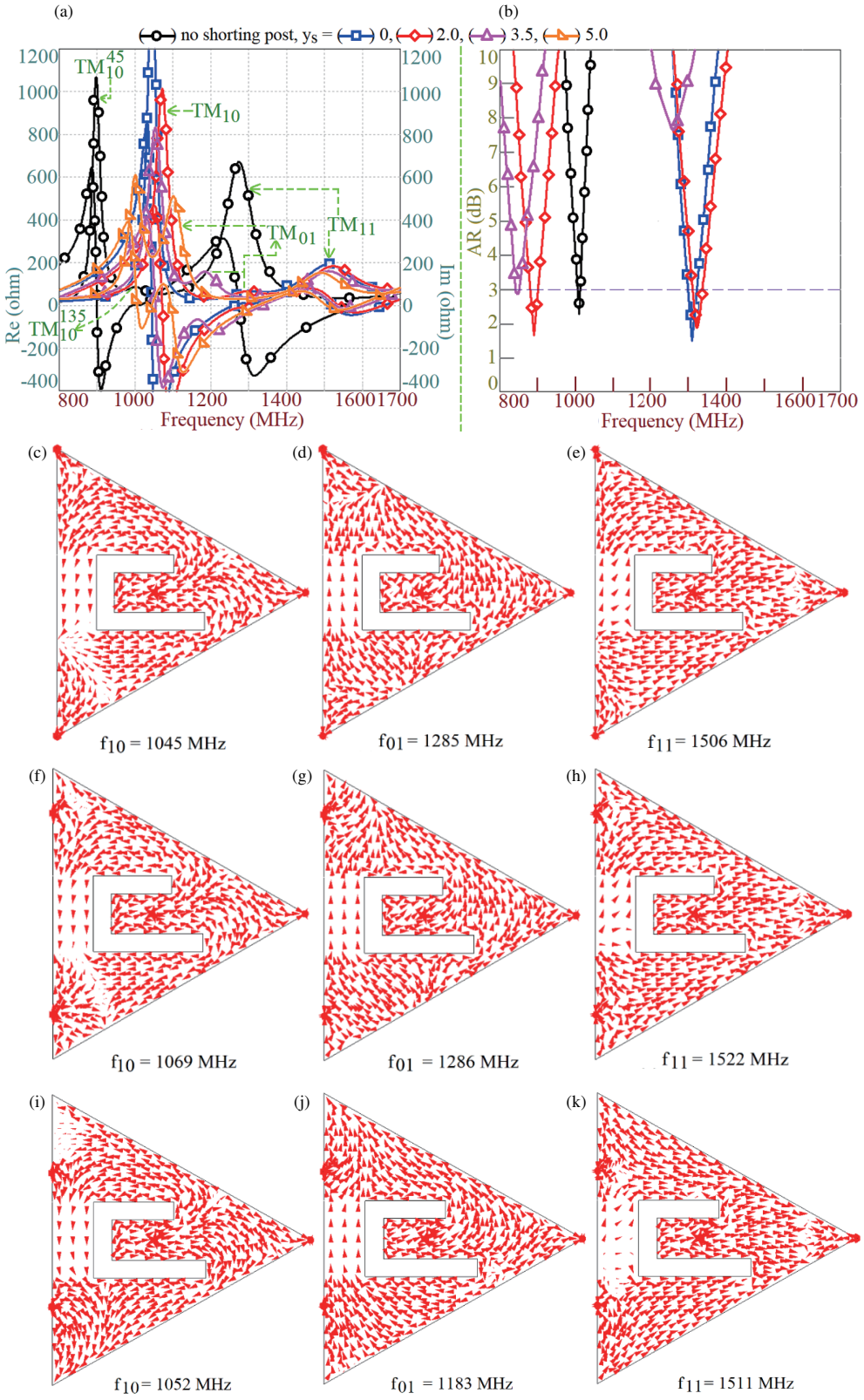

FIGURE 9. (a) Resonance curve and (b) AR plots for variation in shorting posts positions, and surface current distributions at observed resonant modes for y_s = (c)–(e) 0 cm, (f)–(h) 2.0 cm, and (i)–(k) 3.5 cm, for shorted design of U-slot cut ETMSA.

nected, PIN diodes are not forward biased and thus remains in OFF state. This achieves CP response in lower frequency region. With these DC biasing condition, reconfigurable designs are realized, and their response is simulated and experimentally verified. For the above-mentioned antenna parameters, results for these configurations are provided in Figs. 10 and 11. When the PIN diodes are not forward biased, S_{11} BWs observed in the dual bands in the simulation are 73 MHz (7.38%) and 86 MHz

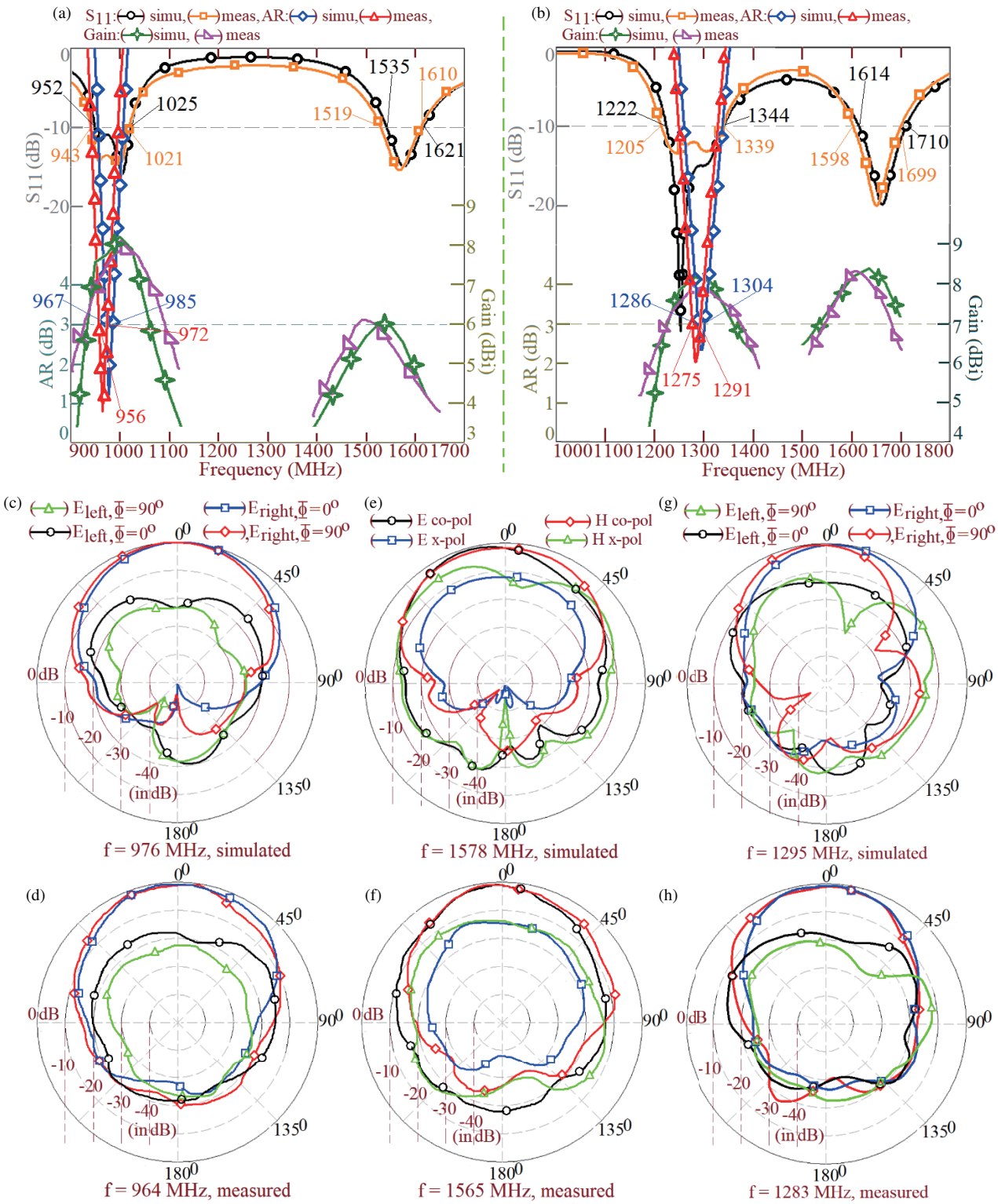

FIGURE 10. Optimum results for (a) OFF and (b) ON state, radiation pattern at the center frequency of (c), (d) AR BW in first band and in (e), (f) second band, for reconfigurable design of shorted U-slot cut ETMSA with diodes in OFF state, radiation pattern at the center frequency of (g), (h) AR BW in first band with diodes in ON state.

(5.45%), respectively. Respective measured S_{11} BWs in the dual bands are 78 MHz (7.94%) and 91 MHz (5.81%), respectively. The AR BWs observed in the first band for simulation and measurement are 18 MHz (1.84%) and 16 MHz (1.65%), respectively. Over the AR BW, peak antenna gain is close to 8 dBic, whereas in the second band peak gain is above 6 dBi.

At the center frequency of AR BW, polarization radiated fields show dominant RHCP wave. Radiation pattern in the second band is in the broadside direction with cross polar level

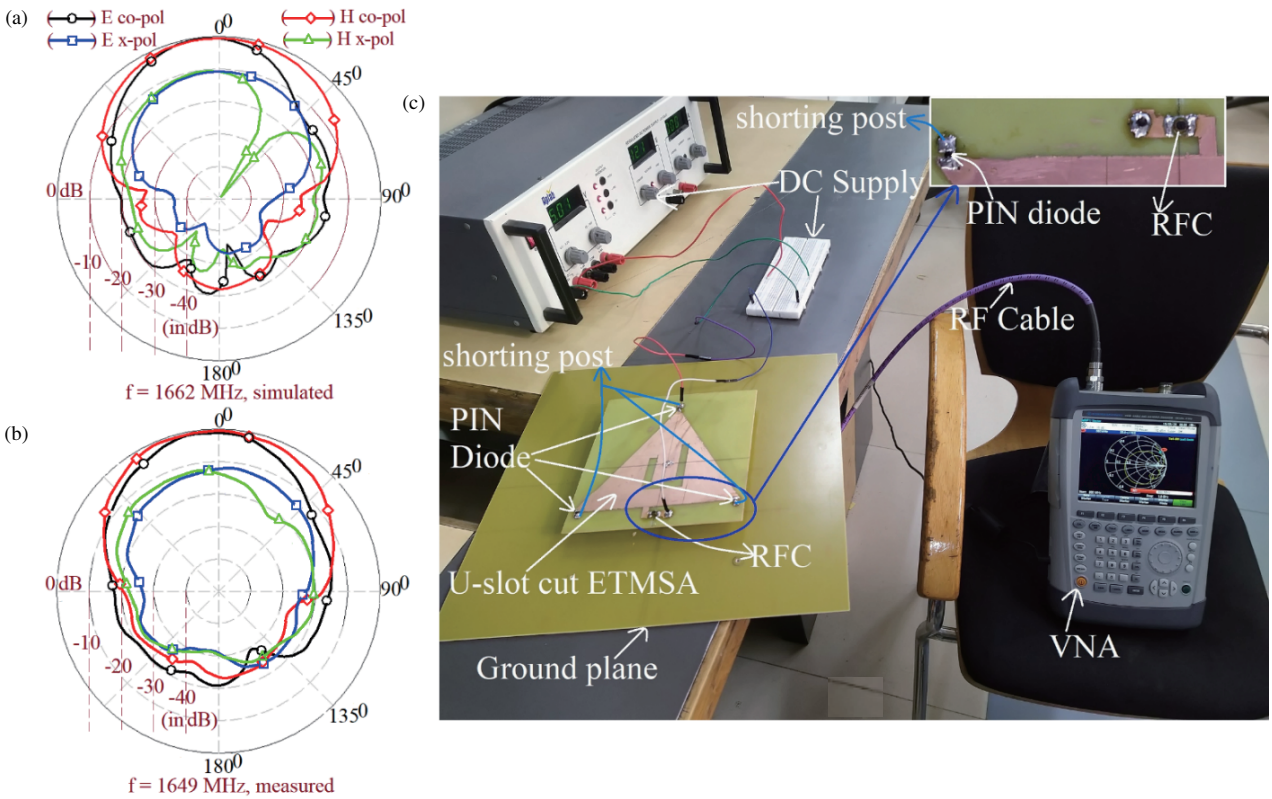

FIGURE 11. Radiation pattern at the center frequency of (a), (b) second band with diodes in ON state, and (c) S_{11} BW measurement setup for reconfigurable design of shorted U-slot cut ETMSA.

less than 10 dB against the co-polar level. The E-plane is aligned along $\phi = 0°$. When the PIN diodes are in ON state, shorting posts are connected to the U-slot cut ETMSA. In this case, S_{11} BWs observed in the dual bands in the simulation are 122 MHz (9.5%) and 96 MHz (5.77%), respectively. Respective S_{11} BW values observed in the dual bands in the measurement are 134 MHz (10.53%) and 101 MHz (6.12%). The AR BWs observed in the first band in the simulation and measurement are 18 MHz (1.38%) and 16 MHz (1.24%), respectively. Over the AR BW in the first band and across the S_{11} BW in the second band, peak antenna gain is close to 8 dBic. With the shorting post loading through the PIN diodes, surface currents at modified TM_{11} mode are unidirectional in variation over the slot cut shorted ETMSA (Fig. 9(e)). This yields increase in the peak gain in the second band, against the design without the loading of shorting posts, where bi-directional current components are observed (Fig. 8(f)). At the center frequency of AR BW, polarization radiated fields show RHCP wave. In the second band, radiation pattern is in the broadside direction with cross-polar level less than 10 dB against the co-polar level with E-plane aligned along $\phi = 0°$. Thus, with reference to the simulated results, with the loading of shorting posts on U-slot cut ETMSA, the center frequency of AR BW increases from 976 MHz to 1295 MHz, thereby giving 319 MHz (32.68%) of frequency tuning. This tuning range is large enough so as to cater to any two frequency bands of wireless application. This tuning option is not reported for earlier designs of U-slot cut ETMSA for CP response. In this regard, reconfigurable designs of U-slot cut CMSA and ETMSA are novel in technique and design. The orthogonal E-field vector magnitude and their phase plots for the reconfigurable shorting posts loaded U-slot cut ETMSA are shown in Figs. 12(a), (b). When the diodes are OFF, the CP response is obtained around 1000 MHz range, as orthogonal E-field magnitudes are nearly equal, and phase component ϕ_x leads ϕ_y by 90°. With the diodes forward biased, orthogonal E-field magnitude is nearly equal around 1300 MHz frequency range, where phase component ϕ_y leads ϕ_x by nearly 270°. These magnitude and phase conditions confirm the presence of RHCP wave in two reconfigurable bands with reference to the antenna as a radiator.

4. DESIGN METHODOLOGY FOR RECONFIGURABLE DESIGN OF SHORTED U-SLOT CUT CMSA

This section initially presents the resonant length formulation for U-slot cut CMSA modes and later presents the design methodology to realize a similar antenna as per specific wireless application. As mentioned above, CP response is due to the degenerated TM_{11} modes. Therefore, first the resonant length formulation for TM_{11} mode and its degenerated variations is presented. While arriving at the resonant length equations for specific mode, parametric variations for specific antenna parameter, as well as the effects of slot dimensions on surface current distribution, are extensively studied. The formulation proposed is explicit for the present design and not referred from any literature. The resonant radial dimension for circular patch

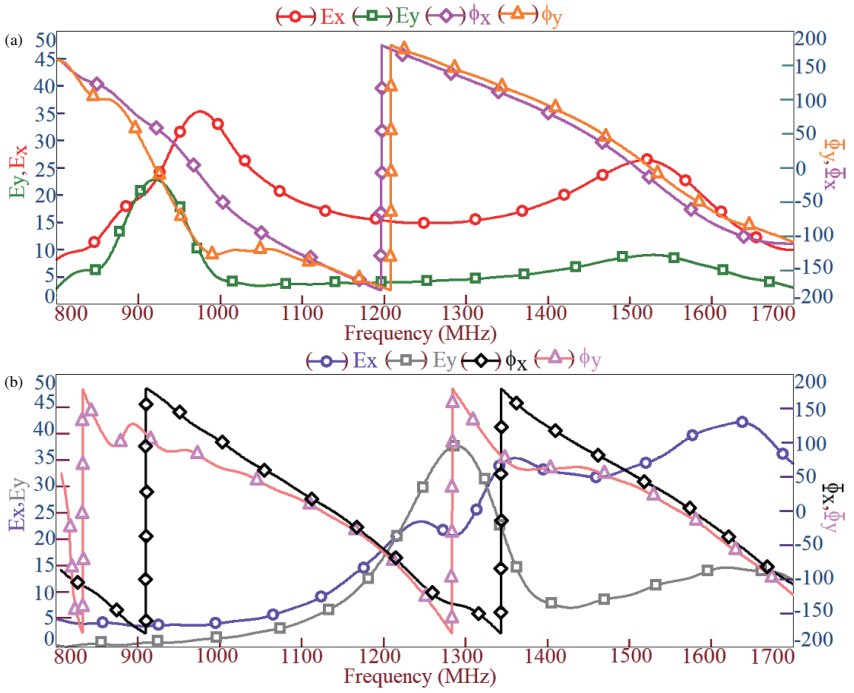

FIGURE 12. Orthogonal E-field magnitude and phase plots for PIN diodes in (a) OFF and (b) ON state for reconfigurable U-slot cut ETMSA.

at TM_{11} mode is given by using Equation (1), and frequency is calculated by using Equation (2). The effective dielectric constant (ε_{re}) is calculated by using Equation (3). For, $r = 6.5$, $h_a = 1.3$, $h = 0.16$ cm, and FR4 substrate, calculated frequency is 956 MHz that closely matches simulated frequency of 949 MHz.

$$r_e = r + 1.1\,(h_a + 2h) \tag{1}$$

$$f_{11} = {K_{mn}c}/{2r_e\pi\sqrt{\varepsilon_{re}}} \tag{2}$$

where, $K_{mn} = 1.84118$ for TM_{11} mode

$$\varepsilon_{re} = \frac{\varepsilon_r^2\,(2h + h_a)}{2h\varepsilon_r + h_a\varepsilon_r^2} \tag{3}$$

Inside the circular patch, an unequal length U-slot is cut. Initially, equal lengths of two horizontal arms of the U-slot are taken, and later one of the arm lengths is increased. The formulation for modified TM_{11} resonant mode, considering the effects of equal horizontal arm U-slot length in addition to vertical U-slot length is proposed first. The vertical U-slot length L_v is not placed near the patch center, where the maximum of TM_{11} modal currents is present. Therefore, L_v has lesser perturbation effects on the TM_{11} modal currents. Hence, separately the effects of L_v on TM_{11} modal currents are not formulated. The modified TM_{11} mode resonant radial dimension considering equal length U-slot effects is formulated by using Equation (4), and the frequency is calculated by using Equation (2) for $r_e = r_{eu}$. For $L_v = 4.0$, $L_h = 4.2$ cm, calculated frequency is found to be 864 MHz that closely matches the simulated frequency of 867 MHz.

$$r_{eu} = r + 1.1\,(h_a + 2h) + \left({L_v}/{20}\right) + \left({L_h}/{6}\right) \tag{4}$$

An unequal length in one of horizontal arms of U-slot degenerates TM_{11} mode into TM_{11}^{45} and TM_{11}^{135} diagonal resonant modes. The TM_{11}^{45} mode frequency decreases with the slot length L_{h1}. The formulation in resonant length for this mode is obtained by using Equation (5). The frequency is calculated by using Equation (2) for $r_e = r_{eu45}$. The calculated frequency is found to be 796 MHz against the simulated value of 798 MHz.

$$r_{eu45} = r + 1.1\,(h_a + 2h) + \left({L_v}/{20}\right) + \left({L_h}/{6}\right) + \left({L_{h1}}/{2.3}\right) \tag{5}$$

Using the above formulations and various resonant mode frequency and antenna dimensional relations existing in the above optimum reconfigurable CMSA, the methodology to design a reconfigurable U-slot cut CMSA as per specific wireless application is presented. Initially, center frequency of the AR BW (f_{cAR}) that represents the CP band without the loading of shorting posts through the RF PIN diodes is selected. Using this frequency, TM_{11} mode frequency of circular patch is calculated as per Equation (6). Further, total substrate thickness h_t is calculated by using Equation (7). In the calculation of h_t, the value of ε_{re} is not available to start with, as air gap thickness (h_a) is unknown. Hence, an initial approximation of $\varepsilon_{re} = 1.2$ is considered. From the calculated value of h_t and for FR4 substrate ($h = 0.16$ cm), h_a is selected that is an integer number. Using these substrate parameters, ε_{re} is recalculated using Equation (3), and the same is used in all further calculations. In all the equations mentioned in the formulation and design methodology section, units of frequency are in GHz, and antenna dimensions are in cm. The circular patch radius for the calculated TM_{11} mode frequency is obtained by using Equation (8).

$$f_{11} = 1.06 f_{cAR} \tag{6}$$

$$h_t = 0.056\left({30}/{f_{cAR}\sqrt{\varepsilon_{re}}}\right) \tag{7}$$

$$r = \left(8.791/f_{11}\sqrt{\varepsilon_{re}}\right) - 1.1\,(h_a + 2h) \quad (8)$$

The modified TM_{11u} mode frequency that considers the effects of vertical U-slot length and two equal arm U-slot lengths bears a frequency ratio $f_{11u} = 0.964 f_{cAR}$, with respect to the center frequency of AR BW. Using this, modified resonant radial dimension (r_{11u}) is calculated as given in Equation (9). Further by rearranging the terms on two sides of Equation (4) and further by using dimensional relation, $L_v = 0.952 L_h$, horizontal U-slot length L_h is calculated as given in Equation (10). The U-slot width is selected as $w_u = 0.19 L_h$.

$$r_{11u} = 8.791/f_{11u}\sqrt{\varepsilon_{re}} \quad (9)$$

$$L_h = r_{11u} - r - 1.1\,(h_a + 2h)/0.2143 \quad (10)$$

An unequal U-slot length L_{h1} degenerates TM_{11u} mode frequency into dual orthogonal diagonally directed resonant modes, and of the two modes (TM_{11}^{45} and TM_{11}^{135}), frequency decreases with an increment in L_{h1}. This frequency bears a frequency ratio $f_{11}^{45} = 0.891 f_{cAR}$ with respect to the center frequency of AR BW as specified above. Using this relation and Equation (11), modified resonant radial dimension r_{11u}^{45} is calculated, and further by using Equation (12), incremental length L_{h1} is obtained. The vertical length in U-slot is placed at a distance of $x_u = 0.677r$ from the circular patch edge, whereas feed point is placed at a distance of $x_f = 0.3846r$ from the open circuit edge of the U-slot, as shown in Fig. 1(a).

$$r_{11u}^{45} = 8.791/f_{11}^{45}\sqrt{\varepsilon_{re}} \quad (11)$$

$$L_{h1} = 2.3\left(r_{11}^{45} - r - 1.1\,(h_a + 2h) + 0.2143 L_h\right) \quad (12)$$

In the reconfigurable U-slot cut CMSA, frequency ratio between the two bands is 1.283 (f_{cAR1}/f_{cAR}). This ratio satisfies the requirement of dual band antenna for GPS L1 and L2 bands. Hence, using the proposed methodology, the procedure to design a reconfigurable U-slot cut CMSA using an FR4 substrate for these two GPS L bands is presented. The $f_{cAR} = 1227$ MHz is selected, and various antenna parameters calculated using the above design methodology are $h_a = 0.9$, $h = 0.16$, $r = 4.7$, $L_h = 2.8$, $L_{h1} = 1.25$, $w_u = 0.5$, $x_u = 3.2$, $x_f = 1.8$ cm. The square shorting pads of length 0.2 cm are placed at an angle of 45° as shown in Fig. 1(c), and a shorting post of wire diameter 0.1 cm is placed. They are connected to the CMSA through PIN diodes, and biasing is provided using the RFC. In the OFF state of PIN diodes, simulated S_{11} BWs observed in dual bands are 76 MHz (6.28%) and 98 MHz (5.6%), respectively. The measured S_{11} BWs noted in the dual bands are 82 MHz (6.4%) and 106 MHz (5.93%), respectively. The simulated and measured values of AR BW observed in the first band are 17 MHz (1.4%) and 19 MHz (1.34%), respectively. The center frequency of AR BW (f_{cAR}) observed in the simulation is 1209 MHz, which is very close to the desired L2 band frequency. The radiation pattern is in the broadside direction over the two bands. The antenna offers peak broadside gain close to 8 dBic in the first band and above 6 dBi in the second band. When the PIN diodes are forward biased, the shorting posts are connected to the patch, and MSA yields CP response in the higher frequency region. For this state, simulated S_{11} BWs observed in dual bands are 145 MHz (9.51%) and 135 MHz (7.39%), respectively. The measured S_{11} BWs noted in the dual bands are 152 MHz (9.81%) and 141 MHz (7.78%), respectively. The simulated and measured values of AR BW observed in the first band are 16 MHz (1.02%) and 15 MHz (0.98%), respectively. The center frequency of AR BW (f_{cAR}) observed in the simulation is 1568 MHz, which is very close to the desired L1 band frequency. Across the two bands, antenna pattern is in the broadside direction with a peak gain of more than 7 dBic. Using the proposed methodology, for some of the antenna parameters non-integer values are obtained. They are rounded off to the nearest possible and practically realizable integer number. Because of this, small variation in results in terms of center frequency of AR BW for L2 and L1 bands are noted. To obtain the result as per the desired frequency, minor parametric optimization in terms of antenna dimensions can be employed. But considering this deviation, proposed design methodology provides guidelines to design slot cut antenna as per specific application with a close match between the desired and simulated/measured results.

5. DESIGN METHODOLOGY FOR RECONFIGURABLE DESIGN OF SHORTED U-SLOT CUT ETMSA

In ETMSA, one half wavelength variation in currents is present along the patch side length, and considering the fringing field extension length, effective side length S_e, at TM_{10} mode is calculated by using Equation (13). The frequency is calculated by using Equation (14). For $S = 13$, $h_t = 1.52$ cm ($h_a = 1.2$, $h = 0.16$ cm), calculated frequency is found to be 1039 MHz that closely matches the simulated frequency of 1041 MHz. The effects of equal lengths of the two horizontal arms of U-slot and vertical U-slot length are added into the effective ETMSA side length as per Equation (15), and the modified TM_{10} mode frequency is calculated by using Equation (14) for $S_e = S_{eu}$. The calculated frequency is found to be 955 MHz against the simulated frequency of 959 MHz.

$$S_e = S + 3\,(h_a + 2h) \quad (13)$$

$$f_{10} = 20/S_e\sqrt{\varepsilon_{re}} \quad (14)$$

$$S_{eu} = S + 3\,(h_a + h) + \left(L_v/35\right) + \left(L_h/2.4\right) \quad (15)$$

An unequal U-slot length (L_{h1}) degenerates TM_{10} mode frequency, and of the two degenerated frequencies, L_{h1} only decreases the TM_{10}^{45} mode frequency as discussed earlier. The formulation in effective side length (S_{eu}^{45}) is realized by using Equation (16). The modified frequency is calculated by using Equation (14) for $S_e = S_{eu}^{45}$. The calculated frequency is found to be 898 MHz against the simulated value of 884 MHz.

$$S_{eu} = S + 3\,(h_a + h) + \left(L_v/35\right) + \left(L_h/2.4\right) + 1.1 L_{h1} \quad (16)$$

The redesign methodology is initiated by specifying the center frequency of the AR BW, f_{cAR}. While using the frequency relation as mentioned in (17), TM_{10} mode frequency of ETMSA

without U-slot and in the presence of shorting posts is calculated. Using Equation (18), the total substrate thickness h_t is evaluated. For this calculation, $\varepsilon_{re} = 1.25$ is selected as the initial approximation. This ε_{re} approximation is as per the substrate parameters present in the above optimum design of U-slot cut ETMSA. From the calculated value of h_t, for FR4 substrate, h_a is selected that is an integer number. The ε_{re} is recalculated using these selected substrate parameters. Patch side length S is calculated by using Equation (19).

$$f_{10} = 1.07 f_{\text{cAR}} \tag{17}$$

$$h_t = 0.054 \left({}^{30}/_{f_{cAR}\sqrt{\varepsilon_{re}}} \right) \tag{18}$$

$$S = \left({}^{20}/_{f_{10}\sqrt{\varepsilon_{re}}} \right) - 3\left(h_a + h\right) \tag{19}$$

An equal horizontal length U-slot of dimensions L_h and L_v reduces the TM_{10} mode frequency. This frequency bears a ratio $f_{10u} = 0.977 f_{cAR}$, with respect to the center frequency of AR BW. Using this and Equation (20), modified patch side length S_{10u} is calculated, and further by using Equation (21), horizontal slot length L_h is evaluated. Equation (21) is obtained while rearranging the terms on two sides of Equation (15) and by using the dimensional relation $L_v = 0.971 L_h$. The U-slot width is selected as $w_u = 0.228 L_h$. An incremental U-slot length L_{h1} reduces the degenerated TM_{10}^{45} mode frequency, and for the optimum design it bears a frequency ratio $f_{10}^{45} = 0.906 f_{cAR}$, with respect to the center frequency of AR BW. The modified patch side length for this frequency is calculated by using Equation (22), and the length L_{h1} is calculated by using Equation (23). Finally, vertical U-slot length is placed at a distance of $x_u = 0.169S$ from the ETMSA base, whereas the feed point is placed at a distance of $x_f = 0.146S$ from the open circuit edge of the U-slot, as shown in Fig. 9(a).

$$S_{10u} = {}^{20}/_{f_{10u}\sqrt{\varepsilon_{re}}} \tag{20}$$

$$L_h = {}^{S_{10u} - S - 3\left(h_a + h\right)}/_{0.444} \tag{21}$$

$$S_{10}^{45} = {}^{20}/_{f_{10}^{45}\sqrt{\varepsilon_{re}}} \tag{22}$$

$$L_{h1} = {}^{S_{10}^{45} - S - 3\left(h_a + h\right) - 0.444 L_h}/_{1.1} \tag{23}$$

In the reconfigurable U-slot cut ETMSA discussed above, frequency ratio between the two bands is 1.326 (f_{cAr1}/f_{cAR}). This ratio satisfies the requirement of dual band antenna for GPS L1 and L5 bands. Hence, using the proposed methodology, the procedure to design a reconfigurable U-slot cut ETMSA using an FR4 substrate for these two GPS L bands is presented. $f_{cAR} = 1176$ MHz is selected, and various antenna parameters calculated using the above design methodology are $h_a = 0.9$, $h = 0.16$, $S = 10.5$, $L_v = 3.0$, $L_h = 3.1$, $L_{h1} = 1.1$, $w_u = 0.7$, $x_u = 1.8$, $x_f = 1.55$ cm. The square shorting pads of length 0.2 cm are placed at each of the vertex points as shown in Fig. 8(c), and shorting posts of wire diameter 0.1 cm are used. These shorting pads are connected to the ETMSA through the PIN diodes, and biasing is provided using the RFC as mentioned in Fig. 8(c). In the OFF state of PIN diodes, simulated S_{11} BWs observed in the dual bands are 100 MHz (8.47%) and 111 MHz (5.89%), respectively. The measured S_{11} BWs noted in the dual bands are 109 MHz (8.8%) and 119 MHz (6.16%), respectively. The simulated and measured values of AR BW observed in the first band are 21 MHz (1.8%) and 19 MHz (1.9%), respectively. The center frequency of AR BW (f_{cAR}) observed in the simulation is 1164 MHz, which is very close to the desired L5 band frequency. The radiation pattern is in the broadside direction over the two bands. The antenna offers peak broadside gain close to 7.5 dBic in the first band and around 5.6 dBi in the second band. When the PIN diodes are forward biased, the shorting posts are connected to the patch, and MSA yields CP response in the higher frequency region. For this diode activation state, simulated S_{11} BWs observed in the dual bands are 152 MHz (9.87%) and 138 MHz (6.94%), respectively. The measured S_{11} BWs noted in the dual bands are 160 MHz (10.3%) and 145 MHz (7.34%), respectively. The simulated and measured values of the AR BW observed in the first band are 37 MHz (2.37%) and 34 MHz (2.45%), respectively. The center frequency of AR BW (f_{cAR1}) observed in the simulation is 1556 MHz, which is very close to the desired L1 band frequency. Across the two bands, antenna pattern is in the broadside direction with a peak gain of more than 6 dBic. The deviation in the values of the center frequency of AR BW from the desired ones is attributed to the non-integer values obtained through the design methodology, which are rounded off to the integer numbers. This introduces some degree of error in the redesign procedure, and thus for the exact L band frequencies, slight parametric optimization for the obtained antenna parameters can be employed.

6. COMPARATIVE ANALYSIS

To put forward the novelty in the proposed study, this section presents the comparative analysis, wherein the results for the proposed designs are compared against the reported narrow band, wideband, and multi-band CP designs, which are obtained using the conventional approach or reconfigurable techniques. It should be noted here that results for the redesigned configurations are not compared in Table 1. The comparison is presented for the measured S_{11} and AR BW against the peak gain and antenna size. For each design mentioned in Table 1, center frequency of AR BW can be evaluated from AR BW and its % value given. As the reported configurations are presented in different frequency ranges and substrate thicknesses, their values mentioned in Table 1 are normalized with respect to the wavelength at the center frequency of AR BW in the first CP band. Further, frequency tuning aspect in CP antennas is also highlighted in the comparative study, as needed in frequency agile applications. The antenna parameters mentioned for the proposed MSAs in Table 1 are for the OFF state of PIN diodes, since it is the initial state, and through the diode activation second band tuning is obtained.

Although the slot cut CP designs discussed [4, 5] and shorted CP MSA discussed in [7] offer comparable values of AR BW, they do not offer frequency tuning for the CP band as needed in frequency agile applications. The slot and stub loaded triple frequency antenna requires large antenna size [6]. Modified ring

TABLE 1. Comparison for proposed reconfigurable MSAs against reported CP MSAs.

MSA shown in	Meas. S_{11} BW (MHz, %)	Meas. AR BW (MHz, %)	Peak Gain (dBi)	Area (A_P/λ^2_{cAR})	Substrate thickness (h_t/λ_{cAR})
Fig. 1(c), CMSA	band 1–68, 7.64 band 2–84, 6.5	band 1–25, 2.82 252 MHz, 28.44% frequency tuning	band 1–7.9 band 2–7.1	0.14	0.055
Fig. 9(c), ETMSA	band 1–78, 7.94 band 2–91, 5.81	band 1–16, 1.65 319 MHz, 33.09% frequency tuning	band 1–8.0 band 2–6.1	0.1	0.053
Ref. [4]	27, 1.71	10, 0.63	5.4	0.14	0.03
Ref. [5]	75, 3.15	40, 1.673	5	0.892	0.02
Ref. [6]	121, 4.99	13, 0.53	7.5	1.512	0.01
Ref. [7]	67, 2.72	16, 0.653	7.6	0.51	0.04
Ref. [8]	—	46, 3.9	3.45	0.41	0.01
Ref. [9]	109, 4.52	26, 1.08	4.62	1.035	0.026
Ref. [10]	30, 1.9	6, 0.4	2.3	0.215	0.05
Ref. [11]	260, 11.2	90, 3.9	9.0	0.12	0.077
Ref. [13]	230, 9.27	230, 9.27	8.3	0.19	0.08
Ref. [14]	810, 35	130, 5.3	9.0	0.21	0.1
Ref. [15]	3600, 62.94	3160, 53.92	3.6	0.457	0.035
Ref. [16]	300, 15.2	160, 8.2	7.0	0.14	0.067
Ref. [17]	1203, 49.29	488, 20.11	7.5	0.32	0.14
Ref. [18]	3080, 63.3	3040, 63.7	17.77	6.2	0.101
Ref. [19]	1570, 28.11	1160, 21.05	8.0	0.15	0.183
Ref. [20]	2000, 40	1000, 19	7.5	0.65	0.12
Ref. [21]	330, 9.36	250, 7.13	7.75	0.67	0.052
Ref. [22]	>5000, 76.92	1200, 23.5	12.0	7.047	0.04
Ref. [23]	322.9, 24.82	520.9, 37.4	4.65	0.735	0.2
Ref. [24]	1800, 40	290, 6.4	2.72	0.11	0.03
Ref. [25]	685, 51.87	band 1–28, 2.24 band 2–69, 4.39	band 1–8.1, band 2–7.2	0.221	0.084
Ref. [26]	band 1: 210, 4.26 band 2: 290, 5.15	band 1: 50, 1.02 band 2: 70, 1.26	band 1: 9.0, band 2: 8.6	2.804	0.047
Ref. [29]	323, 21.98	72, 5.14 (20.6% frequency tuning)	8.0	0.210	0.119
Ref. [30]	618, 42.15	band 1: 49, 4.05 band 2: 61, 3.56	band 1: 7.1, band 2: 3.9	0.1	0.102

shape patch discussed in [8] for GPS applications has lower gain than the proposed design. The modified ground plane structure employing fractal shape geometry discussed in [9] requires higher patch size, whereas U-slot fractal ground plane design discussed in [10] offers lower antenna gain. Resonant U-slot or rectangular slots loaded CP designs discussed in [11–14] do not offer frequency tuning option, which is offered in the proposed configurations. Although the AR BW offered by these designs is higher than the proposed reconfigurable designs, proposed designs are optimized on substrate thickness $\sim 0.055\lambda_{cAR}$, against thicker substrate ($\geq 0.08\lambda_{cAR}$) used in the reported resonant slot cut configurations. A wider AR BW is achieved in the printed monopole antenna, which is loaded with the parasitic elements and backed by offset modified ground plane [15]. However, this design offers lower peak gain and is complex in design and fabrication. Against this, the proposed configuration provides a single patch reconfigurable solution to offer frequency agility. The stacked and gap-coupled designs discussed in [16, 21] offer the AR BW of around 7–8%, which is not large enough to cater to practical wireless applications like GPS L bands. The antenna substrate thickness or patch size is large for the wideband multi-resonator or multiple slots cut CP designs discussed in [17–20]. Antenna dimensions are large for narrow slits cut microstrip line fed design discussed in [22], or patch size, and thickness is higher for wideband CP antenna array discussed in [23]. The dual

band printed patch design discussed in [24] offers lower gain. The dual band design discussed in [25] employs multiple slots and requires a thicker substrate. Against this, the proposed design is a single U-slot cut configuration with smaller substrate thickness. Attributed to the microstrip line feeding the multiple meshed patches, antenna dimensions are higher for the design discussed in [26]. The GPS circular patch antenna discussed in [27] employs four ports with a microstrip line based power divider circuit. All these design features increase the complexity in the reported triple band configuration. Reconfigurable designs discussed in [28–30] exhibit variation in the broadside gain across the frequency tuning range or across the dual bands.

Against the reported CP variations, proposed MSA is simple in design and implementation as it employs single U-slot loaded patch with shorting posts placed in the immediate vicinity. This does not increase the patch area. Loading of shorting posts offers frequency tuning and more than 6 dBic gain across the two bands. This gain is larger than some of the reported dual band CP designs compared above. A coaxial feeding with U-slot is used in the proposed design against the multiple feeds with power divider circuit, for orthogonal mode excitation. The proposed shorting post technique achieves the frequency tuning in single patch U-slot cut CP designs. Although resonant U-slot cut antenna for CP response is the reported configuration, frequency tuning aspect in them is missing, and the same is addressed here. Therefore, in terms of the method used and results obtained for resonant slot cut CP MSAs, proposed work is novel in contribution. The design methodology is presented for the proposed configurations, using which a similar antenna can be redesigned as per specific wireless application, for e.g., GPS L-band designs as discussed above or antennas in Galileo E-band spectrums. Against the reported resonant slot cut CP antennas, AR BW is smaller in the proposed design. However, proposed resonant slot cut antennas are optimized on a substrate thickness of $0.055\lambda_{cAR}$ as against the substrate thickness of more than $0.08\lambda_{cAR}$ used in the reported resonant slot cut antenna. Further, the main thrust of the proposed study is more on exploring the frequency tuning aspect than on the widening of the AR BW in resonant slot cut antennas. On this point, proposed reconfigurable MSA is a better solution against reported resonant slot cut CP MSAs. Considering the practical implementation of proposed design, design methodology presented is useful in realizing similar antennas for practical application that requires frequency ratio of either 1.283 or 1.326, in the two bands. In this regard, as mentioned above, proposed designs are useful to cover GPS L5, L1 and L2, L1 bands. In all the designs, in two reconfigurable states of operation, antenna gain and AR BW in the first band do satisfy the requirement of mentioned GPS L-bands. With frequency ratio of 1.326 between two bands, the triangular patch design is also useful to cover Galileo E1 and E5 bands. Proposed configuration employs a low-cost substrate thus providing a low-cost solution. Further, air suspended configuration is employed that makes the design more reliable in antenna characteristics against the substrate parameter variations. Being fabricated on a thicker lower dielectric constant substrate, antenna dimensions are on the higher side. When the size is a constraint in practical applications, similar designs can be implemented on thinner but efficient microwave substrates having higher dielectric constant. While carrying out the far-field measurements in the reconfigurable designs, DC biasing line will impose problems. Hence, in the far-field measurements either the PIN diodes are replaced by the shorting strips or no connections are made between the patch and shorting posts. The placing of shorting strip is equivalent to the forward bias PIN diode, as it ensures complete connectivity between shorting posts and the patch. In this manner, far-field measurements are carried out in the antenna laboratory.

7. CONCLUSIONS

Reconfigurable variations of U-slot cut CMSA and ETMSA are proposed for frequency tunable CP response. The frequency tuning is achieved with the help of shorting posts loading in the immediate vicinity of the U-slot cut patch. The loading of shorting posts alters the resonant mode distribution on slot cut patch and achieves the frequency tuning for AR BW with a stable gain characteristic. With respect to the initial design, in circular patch U-slot cut antenna, frequency tuning of 28.44% is obtained, whereas equilateral triangular patch design achieves frequency tuning of 33.09%. This frequency tuning feature achieved in resonant slot cut antenna makes them suitable for frequency agile and multi-band applications. The frequency tuning aspect of resonant slot cut antenna is not explored in the reported configurations, and in terms of technique used and results obtained, proposed work is novel in contribution. With the obtained antenna characteristics, redesigned variants of the proposed MSAs are suitable in dual band application pairs like GPS L1, L2 and L1, L5 bands.

REFERENCES

[1] Kumar, G. and K. P. Ray, *Broadband Microstrip Antennas*, Artech House, 2003.

[2] Garg, R., *Microstrip Antenna Design Handbook*, Artech House, 2001.

[3] Wong, K.-L., *Compact and Broadband Microstrip Antennas*, John Wiley & Sons, 2004.

[4] Wang, M.-S., X.-Q. Zhu, Y.-X. Guo, and W. Wu, "Compact circularly polarized patch antenna with wide axial-ratio beamwidth," *IEEE Antennas and Wireless Propagation Letters*, Vol. 17, No. 4, 714–718, 2018.

[5] Bernard, L. B. K., Nasimuddin, and A. Alphones, "AN e-shaped slotted-circular-patch antenna for circularly polarized radiation and radiofrequency energy harvesting," *Microwave and Optical Technology Letters*, Vol. 58, No. 4, 868–875, 2016.

[6] Tan, Q. and F.-C. Chen, "Triband circularly polarized antenna using a single patch," *IEEE Antennas and Wireless Propagation Letters*, Vol. 19, No. 12, 2013–2017, 2020.

[7] Zhang, X., L. Zhu, and N.-W. Liu, "Pin-loaded circularly-polarized patch antennas with wide 3-dB axial ratio beamwidth," *IEEE Transactions on Antennas and Propagation*, Vol. 65, No. 2, 521–528, 2017.

[8] Agrawal, N., A. K. Gautam, and R. Mishra, "Design of low volume circularly polarized annular ring-shaped planar antenna for GPS applications," *International Journal of RF and Microwave Computer-Aided Engineering*, Vol. 31, No. 7, e22698, 2021.

[9] Pandey, S. K., G. P. Pandey, and P. M. Sarun, "Circularly polarized micro-strip antenna with fractal trees loaded ground plane," *Electromagnetics*, Vol. 39, No. 7, 505–523, 2019.

[10] Wei, K., J. Y. Li, L. Wang, R. Xu, and Z. J. Xing, "A new technique to design circularly polarized microstrip antenna by fractal defected ground structure," *IEEE Transactions on Antennas and Propagation*, Vol. 65, No. 7, 3721–3725, 2017.

[11] Lee, K. F., K. M. Luk, W. C. Mok, and P. Nayeri, "Single probe-fed circularly polarized patch antennas with U-slots," *Microwave and Optical Technology Letters*, Vol. 53, No. 6, 1245–1253, 2011.

[12] Chen, Y. and C.-F. Wang, "Characteristic-mode-based improvement of circularly polarized U-slot and E-shaped patch antennas," *IEEE Antennas and Wireless Propagation Letters*, Vol. 11, 1474–1477, 2012.

[13] Khidre, A., K. F. Lee, F. Yang, and A. Elsherbeni, "Wideband circularly polarized E-shaped patch antenna for wireless applications [wireless corner]," *IEEE Antennas and Propagation Magazine*, Vol. 52, No. 5, 219–229, 2010.

[14] Kovitz, J. M., H. Rajagopalan, and Y. Rahmat-Samii, "Circularly polarised half E-shaped patch antenna: A compact and fabrication-friendly design," *IET Microwaves, Antennas & Propagation*, Vol. 10, No. 9, 932–938, 2016.

[15] Midya, M., S. Bhattacharjee, and M. Mitra, "Broadband circularly polarized planar monopole antenna with G-shaped parasitic strip," *IEEE Antennas and Wireless Propagation Letters*, Vol. 18, No. 4, 581–585, 2019.

[16] Cheng, G., B. Huang, Z. Huang, and L. Yang, "A high-gain circularly polarized filtering stacked patch antenna," *IEEE Antennas and Wireless Propagation Letters*, Vol. 22, No. 5, 995–999, 2023.

[17] Deshmukh, A. A., V. A. P. Chavali, and A. G. Ambekar, "Circularly polarized gap-coupled designs of modified square microstrip antennas for WLAN and bluetooth applications," *Progress In Electromagnetics Research C*, Vol. 138, 233–246, 2023.

[18] Verma, A., M. Arrawatia, and G. Kumar, "High gain wideband circularly polarized microstrip antenna array," *IEEE Transactions on Antennas and Propagation*, Vol. 70, No. 11, 11 183–11 187, 2022.

[19] Zeng, J., X. Liang, L. He, F. Guan, F. H. Lin, and J. Zi, "Single-fed triple-mode wideband circularly polarized microstrip antennas using characteristic mode analysis," *IEEE Transactions on Antennas and Propagation*, Vol. 70, No. 2, 846–855, Feb. 2022.

[20] Mondal, T., S. Maity, R. Ghatak, and S. R. B. Chaudhuri, "Design and analysis of a wideband circularly polarised perturbed psi-shaped antenna," *IET Microwaves, Antennas & Propagation*, Vol. 12, No. 9, 1582–1586, 2018.

[21] Wu, Q.-S., X.-Y. Tang, X. Zhang, L. Zhu, G. Zhang, and C.-B. Guo, "Circularly-polarized patch antennas with enhanced bandwidth based on capacitively coupled orthogonal patch radiators," *IEEE Open Journal of Antennas and Propagation*, Vol. 4, 472–483, 2023.

[22] Bui, C. D., N. Nguyen-Trong, and T. K. Nguyen, "A planar dual-band and dual-sense circularly polarized microstrip patch leaky-wave antenna," *IEEE Antennas and Wireless Propagation Letters*, Vol. 19, No. 12, 2162–2166, 2020.

[23] Shokri, M., C. Ghobadi, and J. Nourinia, "Dual-band circularly polarized asymmetric dipole array antenna for GPS L1 and L2 bands," *AEU — International Journal of Electronics and Communications*, Vol. 169, 154753, 2023.

[24] Mondal, K., "Half cutting dual-band circularly polarized monopole antenna for wireless communications," *AEU — International Journal of Electronics and Communications*, Vol. 142, 154012, 2021.

[25] Deshmukh, A. A., T. P. Page, and V. A. P. Chavali, "Dual band circular polarized design of rectangular microstrip antenna for GPS L-band and galileo E-band applications," *Indonesian Journal of Electrical Engineering and Informatics*, Vol. 13, No. 1, 261–276, 2025.

[26] Ta, S. X., K. K. Nguyen, C. Dao-Ngoc, N. Nguyen-Trong, *et al.*, "Single-layer, dual-band, circularly polarized, proximity-fed meshed patch antenna," *IEEE Access*, Vol. 10, 94 560–94 567, 2022.

[27] Smyth, B. P., S. Clark, N. Kannan, and A. K. Iyer, "Compact fully printed GPS/GNSS antenna using embedded MTM-EBGs," *IEEE Transactions on Antennas and Propagation*, Vol. 72, No. 11, 8262–8271, 2024.

[28] Nguyen-Trong, N., L. Hall, and C. Fumeaux, "A frequency- and polarization-reconfigurable stub-loaded microstrip patch antenna," *IEEE Transactions on Antennas and Propagation*, Vol. 63, No. 11, 5235–5240, 2015.

[29] Deshmukh, A. A., H. Mistry, V. A. P. Chavali, A. Viswanathan, and P. Nadkarni, "Reconfigurable designs of sectoral microstrip antennas for single band and tunable circular polarized response," *Progress In Electromagnetics Research B*, Vol. 110, 73–90, 2025.

[30] Deshmukh, A. A., A. Viswanathan, P. Nadkarni, V. A. P. Chavali, and H. Mistry, "Reconfigurable designs of equilateral triangular microstrip antennas for single and dual band circular polarized response in GSM and GPS applications," *AEU — International Journal of Electronics and Communications*, Vol. 193, 155729, Mar. 2025.

[31] CST Software Version 2019.

[32] Toh, B. Y., R. Cahill, and V. F. Fusco, "Understanding and measuring circular polarization," *IEEE Transactions on Education*, Vol. 46, No. 3, 313–318, 2003.

[33] Deshmukh, A. A. and T. P. Page, "Unequal length U-slot cut design of polygon shape microstrip antenna for dual band response," *International Journal of Microwave & Optical Technology*, Vol. 18, No. 2, 153, 2023.